The Canadian Mineralogist
Vol. 49, pp. 1015-1034 (2011)
DOI: 10.3749/canmin.49.4.1015

THE LOW-TEMPERATURE AND HIGH-PRESSURE THERMOELASTIC AND STRUCTURAL PROPERTIES OF CHALCOPYRITE, $CuFeS_2$

KEVIN S. KNIGHT[§]

ISIS Facility, STFC Rutherford Appleton Laboratory, Harwell Science & Innovation Campus, Harwell Oxford, Didcot, Oxon., OX11 0QX, U.K., and Department of Mineralogy, The Natural History Museum, Cromwell Road, London, SW7 5BD, U.K.

WILLIAM G. MARSHALL

ISIS Facility, STFC Rutherford Appleton Laboratory, Harwell Science & Innovation Campus, Harwell Oxford, Didcot, Oxon., OX11 0QX, U.K.

STAN W. ZOCHOWSKI

Department of Physics and Astronomy, University College London, Gower Street, London, WC1E 6BT, U.K.

ABSTRACT

The thermoelastic properties of a sample of chalcopyrite from the Palabora mine, South Africa, have been investigated in the temperature range 4.2 – 330 K at ambient pressure, and between 0.22 and 6.81 GPa at ambient temperature. Magnetization measurements indicated a transition to a second antiferromagnetically ordered phase in the region of 53 K; however, all attempts to characterize this magnetic phase by introducing an ordered moment onto the copper site were unsuccessful owing to the small magnitude of the refined magnetic moment. In agreement with other low-temperature crystallographic measurements made on non-antiferromagnetically ordered adamantine-structured semiconducting materials (group IV; I–VII, II–VI, III–V, I–III–VI_2, II–IV–V_2 compounds), chalcopyrite exhibits negative linear and volumetric thermal expansion over a significant temperature interval. Calculation of the speeds of sound for a number of high-symmetry wave vectors is consistent with Blackman's model for negative thermal expansion. The unit-cell volume and isochoric heat-capacity have been fitted assuming a two-term Debye internal energy function, with consistent values being found for the two characteristic temperatures. The temperature dependence of the thermodynamic Grüneisen parameter shows a deep minimum of ~–3 at T/θ_0 ~0.55 (θ_0 is the Debye temperature at 0 K) and a high-temperature limit of ~0.7; these results are the first demonstration that a chalcopyrite-structured phase behaves in the characteristic manner of the simpler adamantine-structured semiconducting materials. No systematic variation in either the nuclear nor the magnetic structure was found between 4.2 and 330 K, and the vibrational Debye temperatures derived by fitting the temperature dependence of the isotropic atomic displacement parameters show no relationship to features in the phonon density of states function. The bulk modulus of chalcopyrite is 77(2) GPa, in good agreement with that determined by *ab initio* calculations and a recent X-ray-diffraction study, and its pressure derivative is 2.0(6). At high pressure, chalcopyrite remains antiferromagnetically ordered until 6.7(2) GPa, at which point a transition to an amorphous phase is observed. Slow decompression of this phase leads to only a limited recovery of the crystalline phase.

Keywords: chalcopyrite, $CuFeS_2$, magnetization, thermoelastic properties, Grüneisen parameters, negative thermal expansion, neutron diffraction.

SOMMAIRE

Nous avons étudié les propriétés thermoélastiques d'un échantillon de chalcopyrite provenant de la mine Palabora, en Afrique du Sud, sur l'intervalle de température allant de 4.2 à 330 K à pression ambiante, et entre 0.22 et 6.81 GPa à température ambiante. Les mesures de la magnétisation indiquent une transition à une second phase antiferromagnétiquement ordonnée aux environs de 53 K; toutefois, tous nos efforts pour caractériser cette phase magnétique en introduisant un moment ordonné sur le site du cuivre ont été en vain à cause de la faible valeur du moment magnétique affiné. En concordance avec d'autres mesures cristallographiques effectuées sur des matériaux semiconducteurs à structure adamantine et antiferromagnétiquement non ordonnés (composés du groupe IV; I–VII, II–VI, III–V, I–III–VI_2, II–IV–V_2), la chalcopyrite possède une expansion thermique

§ *E-mail address:* kevin.knight@stfc.ac.uk

volumique négative et linéaire sur un intervalle notable de température. Un calcul des vitesses du son pour plusieurs vecteurs d'onde à symétrie élevée concorde avec le modèle de Blackman pour expliquer une expansion thermique négative. Le volume de la maille élémentaire et la capacité calorifique isochorique ont été ajustées en supposant une fonction de l'énergie interne de Debye à deux termes, et nous avons trouvé des valeurs concordantes aux deux températures caractéristiques. La dépendance thermique du paramètre thermodynamique de Grüneisen fait preuve d'un minimum profond d'environ –3 à T/θ_0 environ égal à 0.55 (θ_0 correspond à la température de Debye à 0 K), et d'une limite à haute température d'environ 0.7; il s'agit d'une première démonstration qu'une phase ayant la structure de la chalcopyrite se comporte d'une façon caractéristique des matériaux semiconducteurs à structure adamantine relativement simple. Nous n'avons trouvé aucune variation systématique de la structure nucléaire ou magnétique entre 4.2 et 330 K, et les températures vibrationnelles de Debye dérivées en ajustant la dépendance thermique des paramètres de déplacements atomiques isotropes ne montrent aucune relation avec les attributs de la densité de niveaux de phonons permis. Le module de compressibilité de la chalcopyrite est égal à 77(2) GPa, ce qui concorde bien avec la valeur calculée *ab initio* et les résultats d'une étude récente par diffraction X, et sa dérivée avec la pression serait égale à 2.0(6). A pression élevée, la chalcopyrite demeure antiferromagnétiquement ordonnée jusqu'à 6.7(2) GPa, où il y a transition à une phase amorphe. Une décompression lente de cette phase ne mène qu'à une restauration partielle de la phase cristalline.

(Traduit par la Rédaction)

Mots-clés: chalcopyrite, $CuFeS_2$, magnétisation, propriétés thermoélastiques, paramètres de Grüneisen, expansion thermique négative, diffraction de neutrons.

Introduction

The crystal structure of chalcopyrite, $CuFeS_2$, forms the parent structure-type for a widely studied family of compounds with formula either $A^{I}B^{III}C^{VI}_2$ or $A^{II}B^{IV}C^{V}_2$ (Roman numerals denoting oxidation state), which have been found to exhibit several technologically useful electrical and optical properties. These properties range from semiconductivity in the photovoltaic converter $CuInSe_2$, luminescence in $ZnSiP_2$, piezoelectricity in $CdGeAs_2$, to non-linear dielectric susceptibilities in $AgGaS_2$ (Shay & Wernick 1975, and reference therein). Despite over sixty years of solid-state research, in contrast to the structurally analogous phases, many of the physical properties of $CuFeS_2$ remain contradictory and controversial. For example, the oxidation states of the two anions are still contentious (Todd & Sherman 2003, Todd *et al*. 2003, Mikhlin *et al*. 2005, Pearce *et al*. 2006), and the experimentally derived elastic stiffnesses neither agree with an *ab initio* calculation, nor do they exhibit the expected characteristics for a structure derived from sphalerite, ZnS. Furthermore, both *p*-type and *n*-type conductivity have been measured in different natural single crystals, but the physical and chemical basis for this difference in fundamental transport property remains uncertain (Pridmore & Shuey 1976). Many of these problems can be attributed to the use of relatively uncharacterized natural single-crystal or polycrystalline samples, whereas more detailed studies are exacerbated by the lack of suitable high-purity, synthetic single crystals.

In this paper, we address the thermoelastic properties of a natural sample of chalcopyrite from the Palabora mine, South Africa, using the experimental techniques of powder neutron diffraction at low temperature and high pressure, coupled with measurements of the magnetic field dependence of the magnetization. These new experimental data are supplemented by published data on the heat capacity and *ab initio* calculations of the elastic stiffnesses. In keeping with the current terminology used in solid-state physics, in this paper we have categorized all the crystal structures that can be derived by symmetry descent from the aristotype crystal-structure of diamond, as adamantine structured.

Structural Crystallography and a Review of Physical Properties

Nuclear and magnetic structure, and antiferromagnetic behavior in temperature and pressure

The chalcopyrite structure may be derived from a cation ordering of the zinc site in sphalerite (ZnS) that transforms as the six-dimensional, irreducible representation W_1 (Stokes & Hatch 1988). The resultant lowering of the space-group symmetry from cubic $F\bar{4}3m$ to tetragonal $I\bar{4}2d$ is accompanied by a doubling of the unit-cell *c* dimension and introduces an additional structural degree of freedom, in this case for the x,y coordinate of the anion, which also transforms according to the identical irreducible representation. In the tetragonal structure of chalcopyrite, this displacement pattern arises at the Brillouin zone center from the single, totally symmetric optic mode with irreducible representation A_1, and this mode forms the only unique normal mode of the crystal structure at $\mathbf{k} = \mathbf{0}$. The chalcopyrite structure has two independent four-fold cation positions, ca1 at (0,0,0) (4*a*) and ca2 at (0,0,1/2) (4*b*), with both exhibiting $\bar{4}$ (S_4) point symmetry. The cations are tetrahedrally bonded to four anions, and each cation shows a single cation–anion bond length and two independent, tetrahedral anion – cation – anion bond angles. The anion resides on an eight-fold site (u,1/4,1/8) (8*d*) with point symmetry 2 (C_2) and u ~ ¼, and is bonded to pairs of atoms of both cation types. In addition to the

changes in the polyhedron's bonding parameters (bond lengths and angles) that are related to the magnitudes of both the unit-cell parameters and u, the deviation of u from 1/4 results in a subtle rotation of the constituent polyhedra about [001]. This can be seen to arise from the infinite, corner-sharing nature of the tetrahedral sites in which a rotation about [001] of one ca1 tetrahedron results in a rotation of the opposite sign for the four connected, coplanar ca2 tetrahedra. The bond lengths, bond angles, tetrahedron volumes, quadratic elongations (Robinson *et al*. 1971) and rotation angles of tetrahedra for both cation sites are found to be simple functions of the anion u coordinate and the lattice parameters; these are summarized in Table 1.

At room temperature, $CuFeS_2$ is an antiferromagnetically ordered semiconductor which, according to Harris *et al*. (1997), exhibits magnetic properties more reminiscent of a metal. The Néel temperature is very high, 823 K, and the magnetic susceptibility has been found by Teranishi (1961) to be relatively independent of temperature. The magnetic structure of chalcopyrite has been determined and refined from neutron powder-diffraction data in the Shubnikov group $I\bar{4}2d$ (Donnay *et al*. 1958), with a reduced moment of 3.85 μ_B found for the iron, and a zero moment, within estimated standard deviation, for the copper (Donnay *et al*. 1958). The moment on the iron cation is oriented parallel to the **c** axis, with the moment on the nearest-neighbor iron cation, connected *via* a sulfur anion, aligned in the opposite direction; the magnetic structure derived by Donnay *et al*. (1958) from a natural sample of chalcopyrite is illustrated in Figure 1.

Recently, Woolley *et al*. (1996) challenged the view that the copper ion carries no measurable moment using powder neutron diffractometry and an analysis of magnetic susceptibility data. The latter suggested that an additional magnetic transition occurs in the vicinity of 50 K, and this observation is in accord with discon-

TABLE 1. POLYHEDRON PARAMETERS IN THE CHALCOPYRITE STRUCTURE

	ca1 (0,0,0)	ca2 (0,0,1/2)
Bond length in Å	$\frac{a\sqrt{4+64u^2+(c/a)^2}}{8}$	$a\sqrt{64\left(u-\frac{1}{2}\right)^2+4+(c/a)^2}$
Bond angle 1	$\cos^{-1}\left(\frac{-(c/a)^2}{4+64u^2+(c/a)^2}\right)$	$\cos^{-1}\left(\frac{-(c/a)^2}{4+64\left(u-\frac{1}{2}\right)^2+(c/a)^2}\right)$
Bond angle 2	$\cos^{-1}\left(\frac{-4-64u^2+(c/a)^2}{4+64u^2+(c/a)^2}\right)$	$\cos^{-1}\left(\frac{-4-64\left(u-\frac{1}{2}\right)^2+(c/a)^2}{4+64\left(u-\frac{1}{2}\right)^2+(c/a)^2}\right)$
Tetrahedron volume in Å^3	$\frac{a^2c}{48}\left(8u^2+\frac{1}{2}\right)$	$\frac{a^2c}{48}\left(8u^2-8u+\frac{5}{2}\right)$
Quadratic elongation	$\frac{(16a/c)^{2/3}\left(\frac{1}{4}+4u^2+(c/4a)^2\right)}{3\left(8u^2+\frac{1}{2}\right)^{2/3}}$	$\frac{(16a/c)^{2/3}\left(\frac{1}{4}+4\left(u-\frac{1}{2}\right)^2+(c/4a)^2\right)}{3\left(8u^2-8u+\frac{5}{2}\right)^{2/3}}$
Tetrahedron-rotation angles	$\cos^{-1}\left(\frac{\sqrt{2}\left(2u+\frac{1}{2}\right)}{\sqrt{16u^2+1}}\right)$	$\cos^{-1}\left(\frac{\sqrt{2}\left((1-2u)+\frac{1}{2}\right)}{\sqrt{4(1-2u)^2+1}}\right)$

tinuities found in the intensities of the purely magnetic neutron Bragg intensities for chalcopyrite at around this temperature. The temperature dependence of the lattice parameters was found to show unexpected non-Grüneisen behavior at low temperatures, and, at ~50 K, a marked reduction of both axial thermal expansion coefficients to close to zero was also found. It should, however, be noted that these measurements were carried out on an impure, synthetic sample containing both pyrite (FeS_2) and an unidentified phase which, coincidentally, was only observed in data below 50 K. On the basis of these results, Woolley *et al.* (1996) suggested that the copper atoms order antiferromagnetically below 50 K, with a moment of ~0.05 μ_B oriented antiparallel to neighboring iron cations in the sheets of cations that lie perpendicular to [001]. The resultant changes in the profile-agreement factors on adding the ordered copper moment to the Rietveld analysis were not reported in that study, and hence it is not possible to make any deductions on whether this additional degree of freedom makes a statistically meaningful improvement to the quality of fit to the neutron data. It does remain debateable, however, as to whether powder neutron diffraction would be sensitive to such a small magnitude of the moment in the presence of the large moment associated with the ferric iron.

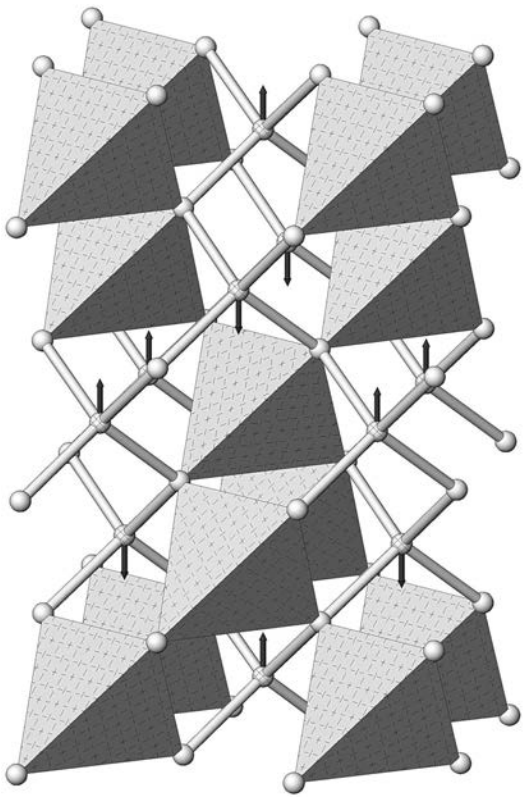

FIG. 1. The nuclear and magnetic structure of chalcopyrite at 300 K viewed down [0.987, 0.173, 0.089] with [–0.323, 0.057, 0.945] vertical. Arrows indicate the moment direction on the ferric ion; the copper site lies within the shaded tetrahedron.

Using a diamond-anvil cell and low-resolution, energy-dispersive X-ray diffraction, Tinoco *et al.* (1994) studied the effect of pressure on the crystal structure of a number of $A^{I}B^{III}C^{VI}_2$ chalcopyrite-structured compounds at ambient temperature. Unfortunately, there is little detail concerning $CuFeS_2$ in their publication beyond a quoted bulk modulus of 91 GPa (with B' = 4) and the observation of a structural phase-transition to a halite-structured (NaCl) phase at a pressure of 7 GPa after a 10% volume reduction. A similar behavior was reported in a more recent angle-dispersive X-ray diffraction and ^{57}Fe resonant inelastic scattering study by Kobayashi *et al.* (2007), who reported a transition at 6.3(0.2) GPa to an amorphous phase, with no indication of a cubic disordered phase at 7 GPa. In their study, the bulk modulus of $CuFeS_2$ for pressures up to 6 GPa was reported to be 69.9(7) GPa (B' = 4). The influence of pressure on the antiferromagnetic ordering of iron in synthetic chalcopyrite has been studied by Vaughan & Tossell (1973) using ^{57}Fe Mössbauer spectroscopy, in conjunction with a diamond-anvil cell. At pressures of 0.5 to 1 GPa, the typical six-peak, Zeeman split spectrum indicative of magnetic ordering was found. With increasing pressure, the sextet was replaced by a broad singlet, and by 1.6 GPa, there was little evidence of any residual magnetic order remaining. In a more recent high-pressure Mössbauer study, Boekema *et al.* (2004) contradicted these results and only found a pressure-independent isomer shift, and no evidence for a magnetic disordering transition to a paramagnetic state below pressures of 2 GPa.

Electrical properties

Both *p*-type and *n*-type conductivity have been measured in different natural single crystals, with a similar low Hall mobility measured for both; 32 $cm^2V^{-1}s^{-1}$ for positive holes (Austin *et al.* 1956), and 35 $cm^2V^{-1}s^{-1}$ for electrons (Teranishi 1961). Thermoelectric measurements made on a number of polycrystalline natural samples were all found to be consistent with *n*-type conductivity (Pridmore & Shuey 1976, Donovan & Reichenbaum 1958), with *p*-type conductivity only found rarely in synthetic samples (Donovan & Reichenbaum 1958). Relatively high carrier concentrations have been measured in chalcopyrite, $10^{18} – 10^{21}$ cm^{-3} (Teranishi 1961, Kradinova *et al.* 1987), but the observed electrical conductivity is anomalously low, which, in the opinion of Mikhailovskii *et al.* (1990), is due to the presence of spin polarons in the antiferromagnetically ordered state. Below 223 K, the conductivity is believed to be extrinsic, governed by impurities, but above 573

K, the conductivity is considered to be intrinsic, and exhibits an irreversible sharp increase (Teranishi 1961, Boltaks & Tarnovskii 1955). As chalcopyrite is known to become increasingly nonstoichiometric on heating (Gorbunova *et al*. 1978, Piekoszewski *et al*. 1968), this irreversible change in conductivity may well be associated with the increasing loss of sulfur at these temperatures. However, in an elegant study of the temperature dependence of the electrical properties of synthetic chalcopyrite between 398 and 873 K, Engin *et al*. (2008, 2011) performed simultaneous measurements of electrical conductivity whilst collecting powder neutron-diffraction data. Experimental results from this study have shown that a semiconductor – metal transition occurs at ~825 K, with the simultaneous loss of long-range magnetic order and disordering of the cations to a sphalerite structure. Under pressure, Pitt & Vyas (1974) found that chalcopyrite undergoes a semiconductor – semiconductor transition at 2.8 GPa and a semiconductor – metal transition at 6.5 GPa, which is close to the pressure reported for the chalcopyrite – rock-salt structural phase transition (Tinoco *et al*. 1994). Neither of these electronic transitions was observed by Boekema *et al*. (2004) in their high-pressure Mössbauer study.

Hamajima *et al*. (1981) calculated the band structure of $CuFeS_2$ in the antiferromagnetically ordered phase using the spin-polarized, self-consistent-charge, discrete-variational $X\alpha$ method. The upper valence bands are constructed from Cu and Fe 3*d* orbitals, with the top of the valence band being at the X point of the tetragonal Brillouin zone. The minimum of the conduction band, composed mainly of Cu and Fe 4*s* and 4*p* orbitals, was at the center of the Brillouin zone, with the calculated energy of the direct gap, 3.1 eV, being in good agreement with experimental determinations of the fundamental absorption-edge energy, 3.2 eV (Oguchi *et al*. 1980). The reduction of the iron moment from that expected for a high-spin Fe^{3+} ion ($^6S_{5/2}$), 5 μ_B, has been attributed by Hamajima *et al*. (1981) to the delocalization of the minority spin *d* electrons that are found to mix strongly into the upper valence-bands.

Elastic properties

Simplistically, the chalcopyrite structure may be considered as a supercell of sphalerite, and hence the elastic stiffnesses would be expected to show the following pseudocubic relationships; $c_{33} \sim c_{11}$, $c_{13} \sim c_{12}$ and $c_{66} \sim c_{44,}$ a prediction that has been confirmed by *ab initio* calculation (Łażewski *et al*. 2004), and experimentally verified in the chalcopyrite-structured phases $CdGeAs_2$ (Hailing *et al*. 1982) and $AgGaSe_2$ (Fouret *et al*. 1997). Despite the availability of suitable natural single crystals, the only experimental measurement of the elastic constants of $CuFeS_2$ have been derived in an indirect method using X-ray diffraction (Sirota & Zhalgasbekova 1991). In this method, the temperature dependence of the intensities of a number of Bragg reflections are analyzed in a Debye formalism, allowing the reflection-dependent vibrational Debye temperatures to be determined. These Debye temperatures are then related to the elastic constants *via* the Christoffel determinant, and the resulting system of equations is solved computationally. In a recent critical review of elastic constants in $A^IB^{III}C^{VI}_2$ and $A^{II}B^{IV}C^{V}_2$ compounds, Neumann (2004) considered the elastic constants of $CuFeS_2$ derived in such a manner to be entirely erroneous, as they are not only inconsistent with the relationships expected in sphalerite, they also disagree with *ab initio* calculations (Łażewski *et al*. 2004), the measured bulk modulus (Tinoco *et al*. 1994) and the Debye temperature determined from heat-capacity measurements (Robie *et al*. 1985).

The unusual thermal expansion behavior correlating with the possible onset of antiferromagnetic ordering of the copper ions (Woolley *et al*. 1996), and the uncertainties in the elastic constants and the pressure-induced semiconductor – semiconductor and semiconductor – metallic phase transitions therefore make a study of the thermoelastic properties of $CuFeS_2$ timely, and of relevance to both mineralogists and solid-state physicists.

Experimental and Data Analysis

Sample

A 15 g sample of chalcopyrite powder was prepared by grinding and subsequent sieving of large, irregular fragments of a natural specimen from the Palabora mine, South Africa. Energy-dispersive X-ray analysis of a representative sample of the specimen showed only the presence of iron, copper and sulfur, with no evidence for chemical impurities. The form of the material was not appropriate for electrical measurements, and hence the nature of the majority carrier is not known for this particular specimen; in a survey of the electrical properties of natural chalcopyrite from a number of localities, however, Pridmore & Shuey (1976) reported only *n*-type conductivity, and furthermore, stated that *p*-type conductivity is more common in synthetic chalcopyrite.

Powder neutron diffraction

Powder neutron-diffraction data were collected on three instruments at the ISIS pulsed neutron source of the Rutherford Appleton Laboratory. High-resolution data were collected on the HRPD diffractometer to determine the magnetic structure at 4.2 K, and the temperature evolution of the unit cell between 4.2 and 330 K. A medium-resolution powder dataset was collected at room temperature on the POLARIS diffractometer to redetermine the room-temperature magnetic structure, and the data to determine the pressure dependence of the unit-cell parameters were collected on the high-flux medium-resolution PEARL beamline.

For the HRPD measurements, 4 cm^3 of powdered and sieved chalcopyrite was lightly packed in an aluminum slab sample can with vanadium front and back windows. All components other than the window materials were masked using gadolinium foil. The sample was cooled to 4.2 K in an AS Scientific "Orange" cryostat under 30 mbar of helium exchange-gas and equilibrated for approximately half an hour. The temperature of the sample can was controlled and monitored by means of a cartridge heater inserted into the wall of the can and a Rh/Fe sensor inserted into the opposite wall. Data were collected in the time-of-flight window 30 ms – 130 ms at 4.2 K, 6 K and in 2 K steps until 70 K, then in 5 K intervals to 330 K. Data were collected for integrated proton currents of 5 μA.hr, approximately 9 minutes in duration at full ISIS beam intensity, and an equilibration step of two minutes was given between each data-collection point once the sample set-point temperature had been reached. The temperature stability was better than ±0.1 K for all measured temperatures. To determine the magnetic structure at 4.2 K, additional datasets were collected in two time-of-flight windows, 30 ms – 130 ms for 400 μA.hr, and 100 ms – 200ms for 200 μA.hr. At each temperature and time-of-flight window setting, a diffraction profile suitable for Rietveld refinement was obtained by electronically focusing the data from the high-resolution back-scattering detector elements to a common *d*-value scale, normalizing the result to the incident distribution of neutron wavelengths from a beam monitor, corrected for detector efficiency and solid angle, and then subtracting the corresponding cryostat background profile.

For the POLARIS measurement, 4 cm^3 of the same $CuFeS_2$ powder used in the HRPD measurements was lightly packed in a cylindrical vanadium sample can 11 mm in diameter, and data were collected at room temperature for 247 μA.hr, approximately 1½ hours. The data from three separate detector banks at $2\theta = 145°$, 90° and 35° were individually focused, background-subtracted, corrected for both the incident distribution of flux and sample self-shielding to generate three powder-diffraction datasets suitable for simultaneous refinement of the profiles.

Ambient-temperature high-pressure data were collected using the $2\theta = 90°$ detectors of the PEARL beamline high-pressure facility (HiPr). About 70 mm^3 of powdered sample material used in the HRPD experiments was loaded into a type-V4a Paris–Edinburgh (P–E) high-pressure cell (Besson *et al.* 1992) equipped with standard profile WC/Ni-binder anvils. The sample was confined between the anvils by means of a single-toroid gasket machined from null-scattering Ti–Zr alloy with fluorinert grade FC–75 used as the pressure-transmitting medium. Oil pressure in the *in situ* ram of the P–E cell was varied using a hand-operated hydraulic pump. A powder-diffraction profile suitable for profile refinement was obtained after focusing the 1080 individual detector-element spectra of the $2\theta = 90°$ bank, normalization of the summed pattern with respect to the incident beam monitor and the scattering from a standard vanadium sample and, finally, a correction for the wavelength and scattering-angle dependence of the neutron attenuation by the anvil (WC) and gasket (TiZr) materials. In the PEARL experiment, we collected diffraction data from two loadings of the P–E cell, the first using a mixed-phase sample of $CuFeS_2$ and NaCl (2:1 by volume) to determine the general compression-induced behavior and the equation of state of chalcopyrite. Here, the sample pressures were derived from the refined NaCl lattice parameter and the room-temperature equation of state of NaCl (Decker 1971). The second P–E cell loading used a pure sample of $CuFeS_2$ to determine the detailed pressure dependence of the crystal structure.

Full-profile Rietveld refinements were carried out using the GSAS package (Larson & Von Dreele 1986).

Magnetization

Magnetization measurements were made in a *Quantum Design* Magnetic Property Measurement System SQUID magnetometer in DC mode. Measurements of the total magnetization of an 8 g sample of $CuFeS_2$, from the same batch used for the neutron-diffraction measurements, as a function of increasing temperature were recorded from 5 to 300 K in applied magnetic fields of 0.1, 0.5 and 2.0 T. The temperature was increased at an average rate of 0.5 K/min.

Results and Discussion

Magnetic susceptibility

The magnetization results are shown in Figure 2. The measurements were made in applied magnetic fields of 0.1, 0.5 and 2.0 T, and in each case a cusp-like anomaly is observed, which suggests the onset of additional antiferromagnetic ordering. The local maxima of these cusps are found to be at the temperatures 55.0 K, 52.6 K and 52.3 K, respectively. The shift of this peak to lower temperatures with increasing applied field is also indicative of an antiferromagnetic ordering. The magnetization results support the previous interpretation of powder neutron-diffraction and magnetic susceptibility data by Woolley *et al.* (1996), that there is an antiferromagnetic ordering of the copper atoms below 50 K.

The temperature dependence of the unit-cell dimensions

The temperature dependence of the lattice parameters for chalcopyrite is shown in Figure 3a, with the temperature variation of the unit-cell volume being shown in Figure 3b. Both crystallographic axes show

the behavior typical of adamantine-structured materials (Barron *et al*. 1980, Barron & White 1999): the lattice parameters are saturated at the lowest temperature, slowly decrease to a minimum with increasing temperature, before exhibiting approximately constant positive thermal expansion at higher temperatures. Similar behavior has previously been observed by Neumann and coworkers in the chalcopyrite-structured compounds $CuInSe_2$ (Deus *et al*. 1983), $CuInTe_2$ (Neumann *et al*. 1984), $ZnSiAs_2$ (Deus *et al*. 1988) and $CuGaTe_2$ (Brühl *et al*. 1981), although none of these studies were carried out for temperatures lower than 30 K, and hence the saturations of the lattice parameters at the lowest temperatures were not observed. The temperatures of the minima for the two axes in chalcopyrite are significantly different, ~86 K for the **a** axis and ~131 K for the **c** axis, and the estimated high-temperature thermal-expansion coefficients derived by extrapolation also show marked differences, 9.0×10^{-6} K^{-1} and 7.2×10^{-6} K^{-1} for α_a and α_c, respectively. Although our magnetic susceptibility data show a small peak at ~52.5 K, similar to that observed by Woolley *et al*. (1996) for their synthetic sample, there is no evidence of a discontinuity or change in slope for either lattice parameter around this temperature. The results presented in Figure 3 bear no resemblance to the limited lattice-parameter data (seven points) shown in Figure 2 of Woolley *et al*. (1996), in which the thermal expansion on both axes appears to be non-Grüneisen in behavior, exhibiting two essentially linear regions, $T < 50$ K, and $50 \text{ K} \le T \le 300$ K. In the first region, the axial thermal-expansion coefficients are large, $\sim 2 \times 10^{-5}$ K^{-1}, whereas in the second region, α_a is a factor of ~20 smaller, and α_c is negligible.

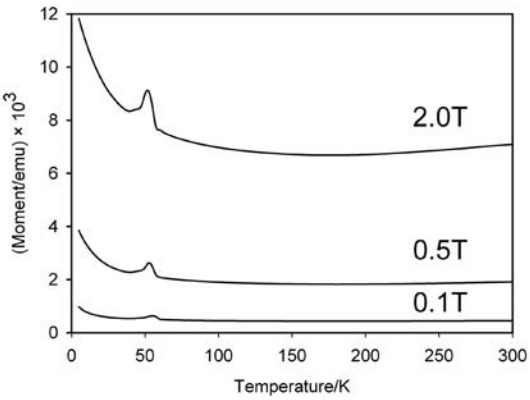

FIG. 2. The temperature dependence of the magnetization of chalcopyrite (~8 g) in applied magnetic fields of 0.1, 0.5 and 2.0 T. The temperature was increased at an average rate of 0.5 K/min. The anomaly near 55 K in each set of data is indicative of a small antiferromagnetic transition identified by Woolley *et al*. (1996) as the ordering of the copper magnetic moments.

As the time-of-flight data were collected at fixed sample and detector positions, we have no explanation for the discrepancy between our measurements and those of Woolley *et al*. (1996) unless there is a severe, uncorrected and temperature-dependent zero-error associated with their reactor-derived powder-diffraction data.

A negative volume or linear expansion, although apparently counterintuitive, is in fact a common phenomenon and has been exploited technologically in applications as diverse as astronomical telescope mirrors to oven-to-table cookware. Standard thermodynamic transformations (Wallace 1972) give the volume thermal expansion coefficient α_V in terms of the isothermal compressibility χ_T and the entropy S:

$$\alpha_V = \left(\frac{\partial \ln V}{\partial T}\right)_P = \chi_T \left(\frac{\partial S}{\partial V}\right)_T .$$

As the isothermal compressibility is positive for thermodynamic stability (Wallace 1972), the change in volume on heating will always be in the direction of increasing entropy. The thermodynamic Grüneisen parameter γ^{th} is related to α_V through the heat capacity at constant volume, C_V, and the isothermal bulk modulus, K_T:

$$\gamma^{th} = \alpha_V V K_T / C_V = \chi_T \left(\frac{\partial S}{\partial T}\right)_T VK_T \Big/ C_V$$

and should equal a weighted average of individual phonon-mode Grüneisen parameters (Wallace 1972):

$$\gamma^{th} = \sum_i C_i \gamma_i \Big/ \sum_i C_i , \quad \gamma_i = -d \ln \omega_i / d \ln V$$

where ω_i is the frequency of mode i, and C_i, its contribution to the heat capacity at constant volume. Thermal expansion will therefore be negative if the excitation of a sufficient number of highly weighted modes with negative (*i.e.*, soft) mode Grüneisen parameters outweighs those excited modes with positive Grüneisen parameters (Barrera *et al*. 2005).

The presence of negative thermal expansion at low temperatures is a characteristic of the adamantine-structured semiconductors (Barron *et al*. 1980, and references therein, Barron & White 1999) and was predicted in the sphalerite structure by Blackman (1958) even before any detailed experimental studies had been carried out. Earlier theoretical work by Barron (1957) had shown that for negative thermal expansion in simple crystal structures to exist, it was a necessary prerequisite for there to be a component of motion transverse to the bond direction. Blackman (1958) concluded that negative thermal expansion is to be expected from open structures and, in particular, those with relatively low shear moduli would be favored. At low temperatures,

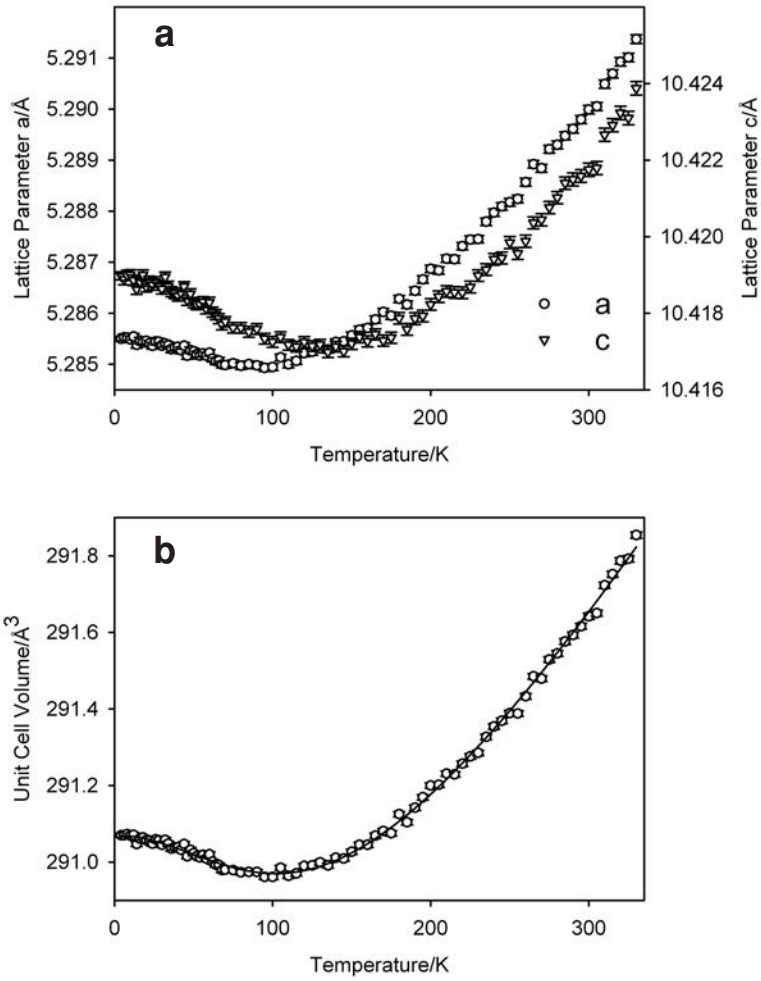

FIG. 3. a. The temperature dependence of the lattice parameters of chalcopyrite showing the characteristic behavior of adamantine-structured compounds. At the lowest temperatures, the lattice parameters are saturated before undergoing negative linear thermal expansion to a shallow minimum with increasing temperature, and finally exhibiting positive high-temperature thermal expansion. b. The temperature dependence of the unit-cell volume and the fit to these data using a two Debye-moment model as described in the text.

only the long wavelength ($\mathbf{k} \sim \mathbf{0}$) acoustic modes are excited, and low shear moduli indicate correspondingly low frequencies for the transverse acoustic (TA) modes. Blackman (1958) showed that in the sphalerite structure, for any reasonable interatomic potential, the TA mode with wavevector [110], polarization [1$\bar{1}$0], and speed $\sqrt{(c_{11} - c_{12})/2\rho}$ would have a strongly negative-mode Grüneisen parameter.

In the chalcopyrite structure, the situation is more complex owing to the unit cell doubling along **c**, and the twelve symmetry-equivalent <110> directions in sphalerite become two groups in chalcopyrite, one of multiplicity four, <110>, and one of multiplicity eight, <201> (making the simplifying assumption $c = 2a$). Considering the <110> group first, for the wavevector [110], two transverse waves with displacement eigenvectors [1$\bar{1}$0] and [001] are found as the solutions to the Christoffel equation (Grimvall 1999). At $\mathbf{k} = \mathbf{0}$, the twenty-four phonon branches decompose according to the irreducible representations

$\Gamma_{opt} = 1A_1 + 2A_2 + 3B_1 + 3B_2 + 6E$

$\Gamma_{ac} = 1B_2 + 1E$

for the optic and acoustic modes, respectively (Fateley *et al*. 1972). Application of projection-operator techniques shows that a linear combination of atomic displacements associated with the E acoustic mode has a polarization in $[1\bar{1}0]$, and hence, we identify this mode as the TA mode in chalcopyrite, which is the equivalent to the TA mode first identified by Blackman as the source of the negative thermal-expansion coefficient in sphalerite. It is highly probable that many other modes away from $\mathbf{k} = \mathbf{0}$ exist that are also associated with negative Grüneisen parameters; however, these would require determination from *ab initio* calculation, and hence are beyond the scope of this paper.

In Table 2, we show the product of density × speed^2 for the longitudinal and two transverse waves with wavevector [110], using Voigt notation for the elastic stiffnesses. If chalcopyrite exhibited the elastic properties of a cubic material, then these values would be identical to those of sphalerite, which for completeness are also shown in the table. Furthermore, if we make the simplifying assumption $c = 2a$, the identical calculation can be carried out for the group of directions <201>. For the [201] wavevector, the wave with displacement eigenvector [010] is purely transverse, whereas the remaining two modes are quasi-longitudinal and quasi-transverse in character. The quasi-transverse mode with polarization vector ~$[10\bar{2}]$ essentially corresponds to the nature of the [110] TA mode; we predict that this mode will also have a negative-mode Grüneisen parameter. In Table 2, we show the product of density × speed^2 for the three modes associated with this wavevector. As before, if chalcopyrite were elastically cubic ($c_{33} = c_{11}$, $c_{13} = c_{12}$ and $c_{66} = c_{44}$), A and B would be ±1, respectively, and the density × speed^2 for the three modes would be identical to those of sphalerite.

Assuming that the calculated elastic constants of Łażewski *et al*. (2004) are correct, the wave speeds for the significant directions in chalcopyrite can be calculated, and these are summarized in Table 3 for the wavevectors [100], [001], [110] and [201]. From the tabulated results, we can see that the speeds of the TA mode, with wave vector [110], and the quasi-transverse mode, with wave vector [201], are both low, and would hence be likely to have correspondingly low frequencies. The difference in the temperature of the minimum in the two lattice parameters would also suggest that the mode(s) relating to the negative thermal expansion have different energies for the two axes, with those for the **c** axis having lower velocities. This view is upheld by the work of Harris *et al*. (1997), in which the acoustic phonons propagating in [110] have been found to have significantly higher velocities than those propagating in [001].

The temperature variation of the tetragonal distortion parameter Δ ($\Delta = 2 - c/a$) is less sensitive to the presence of the local minima in the lattice-parameter variation and shows a relatively simple temperature-dependence: saturation for T < 50 K and an approximately linear increase with increasing temperature for T > 100 K. Further evidence for the atypical physical behavior of $CuFeS_2$ can be found by comparing Δ(T) with other $CuB^{III}C^{VI}_2$ chalcopyrite-structured compounds. For

TABLE 2. DENSITY × ACOUSTIC VELOCITY^2 IN SPHALERITE AND CHALCOPYRITE

	Longitudinal mode in GPa	Transverse mode in GPa, positive Grüneisen parameter	Transverse mode in GPa, negative Grüneisen parameter
sphalerite [110] wavevector	$\frac{c_{11}+c_{12}+2c_{44}}{2}$	c_{44}	$\frac{c_{11}-c_{12}}{2}$
chalcopyrite [110] wavevector	$\frac{c_{11}+c_{12}+2c_{66}}{2}$	c_{44}	$\frac{c_{11}-c_{12}}{2}$
chalcopyrite [201] wavevector*	$\frac{(c_{11}+c_{44})+(c_{13}+c_{44})A}{2}$	$\frac{c_{44}+c_{66}}{2}$	$\frac{(c_{11}+c_{44})+(c_{13}+c_{44})B}{2}$

* assuming the lattice parameters are related by $c = 2a$. $A = \frac{-(c_{11}-c_{33})}{2(c_{13}+c_{44})} + \sqrt{\frac{(c_{11}-c_{33})^2}{4(c_{13}+c_{44})^2}+1}$

$B = \frac{-(c_{11}-c_{33})}{2(c_{13}+c_{44})} - \sqrt{\frac{(c_{11}-c_{33})^2}{4(c_{13}+c_{44})^2}+1}$

room-temperature measurements, Brühl *et al.* (1981) found, to a very good approximation, $1/\Delta\ d\Delta/dT = 4 \times 10^{-4}\ K^{-1}$, for B = (Al, Ga, In) and C = (S, Se, Te). At 300 K, $CuFeS_2$ plots far off this common line with $1/\Delta\ d\Delta/dT = 1.7 \times 10^{-4}\ K^{-1}$, a value that lies closer to a similar curve determined for the $A^{II}B^{IV}C^{V}_2$ compounds, for which $1/\Delta\ d\Delta/dT \approx 1.1 \times 10^{-4}\ K^{-1}$ (Neumann 1980).

The temperature dependence of the unit-cell volume

The temperature variation of the unit-cell volume (Fig. 3b) shows the same features as the unit-cell edges, namely saturation at the lowest temperatures, T < 25 K, a region of negative volume-expansion to a shallow minimum, 25 K < T < 101 K, and finally a region of positive thermal expansion that slowly increases to a constant value of $25.0 \times 10^{-6}\ K^{-1}$ by 300 K. In their work on the thermal expansion of $CuInSe_2$, $CuInTe_2$, $CuGaTe_2$ and $ZnSiAs_2$, Neumann and co-workers fitted the temperature dependence of the lattice parameters to an empirical quartic function of temperature (Deus *et al.* 1983, 1988, Neumann *et al.* 1984, Brühl *et al.* 1981). However, by fitting the temperature variation of the unit cell to simple statistical mechanical models, it is possible to derive useful thermodynamic properties for a wide variety of terrestrial and planetary materials (Knight & Price 2008, Brand *et al.* 2009, Knight & Henderson 2007, Fortes *et al.* 2005, 2006, Wood *et al.* 2002, 2004). If a Grüneisen approximation for the zero-pressure equation of state is assumed, the effects of thermal expansion are considered to be equivalent to elastic strain (Wallace 1972). For low-temperature data with only a limited range in temperature, as in this study, the volume scales with the internal energy U(T), and to first order,

$$V_T = V_0 + \frac{\gamma' U(T)}{K_0}$$

where γ' is a Grüneisen parameter, K_0 is the isothermal bulk modulus, and V_0 is the volume at 0 K. To account for the negative volume-expansion coefficient, it is clearly necessary to modify this expression to allow for two separate Grüneisen parameters of opposite sign, each associated with its own internal energy function. For simplicity in fitting the unit-cell volume data, the internal energies $U_{1,2}(T)$ may be calculated using either an Einstein formulation:

$$U_{1,2}(T) = \frac{3Nh\omega_{E1,2}}{e^{h\omega_{E1,2}/k_BT} - 1}$$

or the Debye formulation:

$$U_{1,2}(T) = 9\,Nk_BT\left(\frac{T}{\theta_{D1,2}}\right)^3 \int_0^{\theta_{D1,2}/T} \frac{x^3 dx}{e^x - 1},$$

where N is the number of atoms in the unit cell, k_B is Boltzmann's constant, θ_D is the Debye temperature and the Einstein temperature, θ_E, is $h\omega_E/k_B$. For consistency, the contributions of the two internal energy functions were fixed to the values found from fitting the data on heat capacity to two Debye moments (see a later section for details). Both approximations gave essentially indistinguishable fits to the unit-cell volume data, with Figure 3b showing the results of fitting the data to the Debye model. The results of the weighed least-squares fitting gave: $V_0 = 291.0681(4)$ Å^3, $\theta_{E1} = 497(16)$ K, $\gamma_1'/K_0 = 2.12(7) \times 10^{-11}$ Pa^{-1}, $\theta_{E2} = 51(16)$ K and $\gamma_2'/K_0 = -7.0(3) \times 10^{-12}$ Pa^{-1} for the Einstein approximation to the vibrational density of states, and $V_0 = 291.064(3)$ Å^3, $\theta_{D1} = 647(31)$ K and $\gamma_1'/K_0 = 2.35(6) \times 10^{-11}$ Pa^{-1}, $\theta_{D2} = 111(23)$ K and $\gamma_2'/K_0 = -1.0(1) \times 10^{-11}$ Pa^{-1} for the Debye approximation to the phonon density of states. With an experimentally determined bulk modulus of 77(2) GPa (see a later section for details), γ_1' is equal to 1.63(7), and γ_2', to –0.54(3) in the Einstein approximation, and γ_1' is equal to 1.81(6), and γ_2', to –0.77(8) in the Debye approximation.

Temperature dependence of the structural parameters

No evidence was found from the Rietveld fit to the HRPD and POLARIS data for the coexistence of a tetragonal and cubic chalcopyrite phase that was recently claimed for a specimen from Rio Grande do Sul, Brazil (Mussel *et al.* 2007). Throughout the whole temperature-interval from 4.2 to 300 K, the anion coordinate showed a negligible variation with temperature, with an average value of 0.252(1), this apparently large estimated standard deviation being associated with both the short data-collection times and the small magnitude of the neutron scattering cross-section of sulfur. More precise structural parameters were determined from the room-temperature POLARIS data and the HRPD data collected at 4.2 K and are listed in Table 4 with the

TABLE 3. SOUND VELOCITIES IN CHALCOPYRITE BASED ON THE CALCULATED ELASTIC STIFFNESSES OF ŁAŻEWSKI *et al.* (2004)

Wavevector	Character	Displacement	Speed km s^{-1}
[100]	Longitudinal	[100]	4.635
[100]	Transverse	[010]	2.579
[100]	Transverse	[001]	2.470
[001]	Longitudinal	[001]	4.745
[001]	Transverse	[100], [010]	2.579
[110]	Longitudinal	[110]	4.972
[110]	Transverse	[1$\bar{1}$0]	1.846
[110]	Transverse	[001]	2.470
[201]	Quasi-longitudinal	~[201]	5.010
[201]	Transverse	[010]	2.525
[201]	Quasi-transverse	~[10$\bar{2}$]	1.730

fits to the simultaneous three-bank refinement of the POLARIS data shown in Figure 4. Within the estimated standard deviation, the polyhedron's parameters listed in Table 1 are temperature-invariant; however, there exist significant differences between the two cation tetrahedra. The CuS_4 tetrahedron has a larger volume at all temperatures [mean: 6.11(4) Å^3)] than the FeS_4 tetrahedron [mean: 6.02(4) Å^3], and is more distorted, with larger quadratic elongation and tetrahedron angle variance (Robinson *et al*. 1971). Both tetrahedra exhibit one pair of bond angles greater than the ideal tetrahedron angle and one smaller, with the deviations of the two bond angles from the ideal tetrahedron angle being smaller for the FeS_4 tetrahedron.

The temperature dependence of the atomic displacement parameters derived from the rapid HRPD data collections have been analyzed using the modified Debye formalism of Wood *et al*. (2002), in which the zero-point displacement is allowed to be an additional refineable parameter. The fits to the displacement parameters are shown as full lines on Figure 5a–c with refined vibrational Debye temperatures of 206(2) K, 242(3) K and 333(12) K found for the iron, copper and sulfur, respectively. The magnitudes of the isotropic atomic displacement-parameters at 300 K are in good agreement with the isotropic equivalent displacement parameters derived from *ab initio* calculations (Łażewski *et al*. 2004); however, these vibrational Debye temperatures show no correlation with features in the calculated total, or partial phonon density of states.

At room temperature, the magnetic structure of Donnay *et al*. (1958) was confirmed with a refined moment of 3.23(1) μ_B for the iron and a zero moment, within estimated standard deviation, for the copper. The HRPD data were collected at a significantly lower temperature than the temperature observed for the anomaly in the magnetic susceptibility, and hence might be expected to show evidence for ordering of the copper ion, as suggested by the work of Woolley *et al*. (1996). However, an identical result to the room-temperature refinement was found, and the introduction of a moment on the copper site gave no statistically meaningful improvement to the quality of fit to the data. Furthermore, the integrated intensities of "magnetic only" reflections, normalized to a neighboring "nuclear only reflection", showed no evidence for the discontinuities observed by Woolley *et al*. (1996). We can therefore neither confirm nor deny the low-temperature magnetic structure proposed by Woolley *et al*. (1996), with our refined copper moment invariably within one or two estimated standard deviations of zero magnitude. It could possibly be argued that we see some evidence for the ordering of the copper ion inasmuch as the moment direction invariably refined to be antiparallel to the moment orientation of the neighboring iron, irrespective of the starting orientation. It is clear, however, that a direct confirmation of the ordering of the copper site would be better carried out using an element-specific probe; powder neutron diffraction is too insensitive to the potentially small moment carried by the copper ion.

TABLE 4. STRUCTURAL PARAMETERS FOR CHALCOPYRITE AT 300 AND 4.2 K

	300 K	4.2 K
a in Å	5.2900(1)	5.28563(1)
c in Å	10.4217(2)	10.41917(2)
Fe U_{iso} in Å^2	0.0097(2)	0.0049(2)
Fe moment in μ_B	3.23(1)	3.57(1)
Cu U_{iso} in Å^2	0.0161(3)	0.0048(3)
S U	0.2604(7)	0.2529(8)
S U_{iso} in Å^2	0.0084(2)	0.0053(2)

Heat-capacity measurements and fitting

The isobaric (C_P) molar heat-capacity of synthetic $CuFeS_2$ has been reported by Robie *et al*. (1985) in the temperature interval from 5.38 to 303.54 K. Although the difference between the isochoric (C_V) and isobaric heat capacities is small at low temperatures ($C_V - C_P = -TK_0\alpha^2V_m$; molar volume, V_m, volume thermal expansion coefficient, α, bulk modulus K_0), in the fitting of the heat-capacity data to Debye models, we have converted the C_P data to C_V using results from fitting the unit-cell volume as a function of temperature and pressure. The converted heat-capacity data are shown plotted in Figure 6. For a Debye density of states function, the isochoric heat-capacity varies as a function of temperature as

$$C_V(T) = 9Nk_BT\left(\frac{T}{\theta_D}\right)^3 \int_0^{\theta_D/T} \frac{x^4 e^x dx}{\left(e^x - 1\right)^2}$$

(Wallace 1972, Grimvall 1999). The dashed line in Figure 6 shows the results of a least-squares fit to the heat-capacity data according to this model, with a fitted Debye temperature of 362(6) K. It is quite evident from the figure that this is a poor approximation to the measured heat-capacity; at the lowest and at the highest temperatures measured, there are more excited modes than the model predicts, whereas in the intermediate temperature interval, the opposite effect is found. Modifying the model to take account of these observations, the data were refitted using an equal weighting of two Debye moments and the assumption of Dulong–Petit behavior at a high temperature. The fit to the data in this case was significantly better, and this was found to be further improved by removing the assumption of a high-temperature limit of 3NR and equal weighting of the two Debye moments. We justify the former on the pragmatic grounds that, in the absence of measurements of the spin-wave dispersion curves for $CuFeS_2$

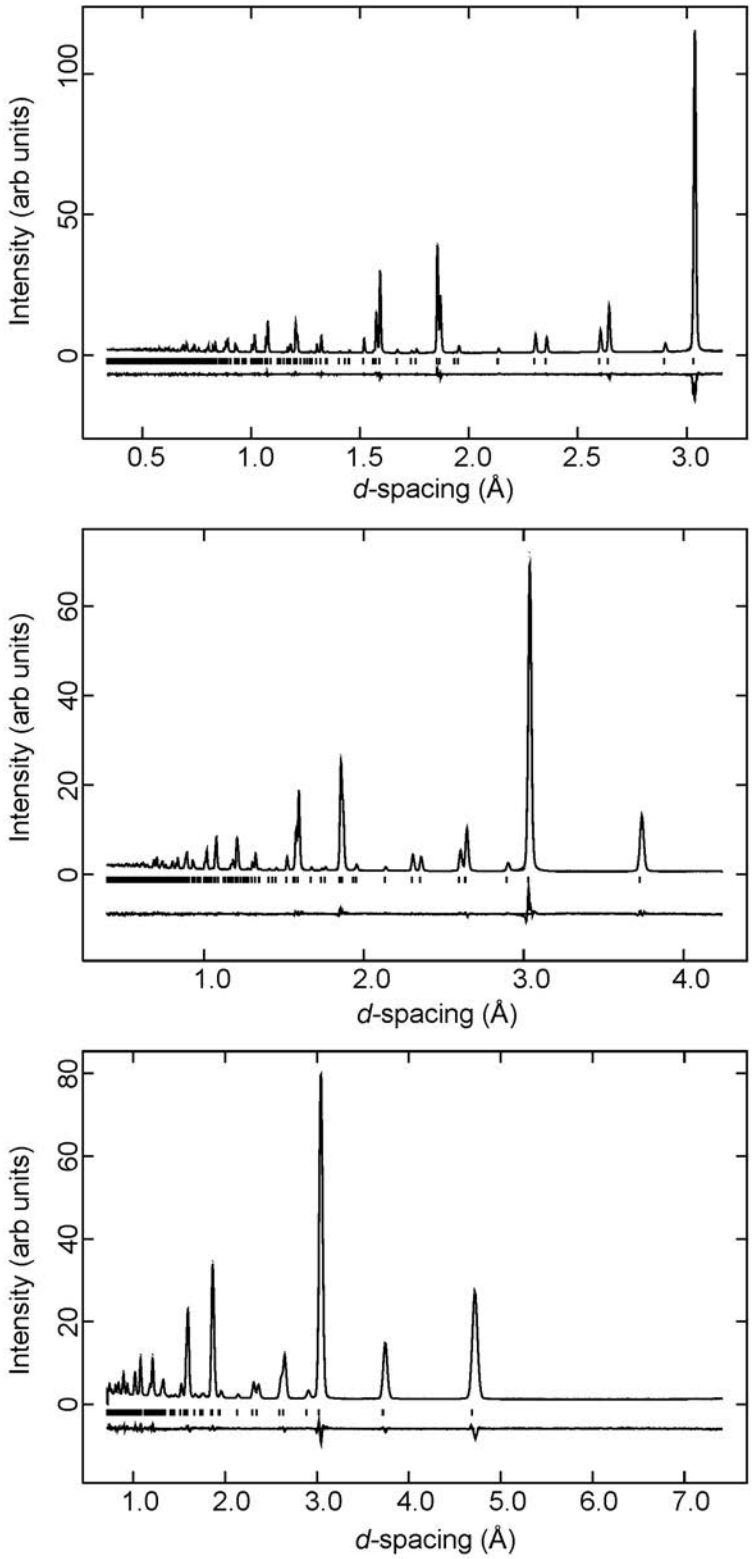

FIG. 4. Final Rietveld refinement plots for the 300 K data collected on the POLARIS diffractometer. Upper plot is for 2θ = 145°, middle for 2θ = 90° and lower for 2θ = 35°. In all three plots, the difference curve represents observed – calculated intensity.

that would allow a more sophisticated heat-capacity expression to be developed, the additional contribution to the heat capacity from antiferromagnetic order is similar to that of the lattice contribution (Gopal 1966).

The fitted Debye temperatures 167(2) K and 601(5) K are reasonably close to the values determined from fitting the volume expansion (111 K, 647 K), thus giving some confidence to the method of analysis. An alternative fit of the data using two Einstein heat-capacity functions gave characteristic temperatures of 117(2) and 445(6) K, which correspond to characteristic frequencies of vibration of 2.44 and 9.27 THz, respectively. The calculated total and partial phonon densities of states (Łażewski *et al*. 2004) are plotted in Figure 7 from data kindly provided by Dr. Jan Łażewski (Institute of Nuclear Physics, Cracow). The former is characterized by the presence of three broad groups of peaks centered on 2.1 THz, 5.0 THz and 9.1 THz, with a gap in the density of states function between middle and the highest frequency-groups. The lowest frequency-group corresponds to modes mostly involving copper, whereas the highest frequency-group is dominated by the contributions from the iron and sulfur alone, and it is these two bands that dominate the total phonon density of states. The mid-points of both of these bands of modes can be seen to be gratifyingly close to the values derived from the fitting of the heat-capacity data to the simple optic-mode Einstein model.

High-pressure behavior

Figure 8 shows the neutron powder-diffraction patterns obtained from the mixed-phase P-E cell loading of $CuFeS_2$ and NaCl. From bottom to top, the patterns are shown in the order collected, with all except the final pattern being collected with increasing applied cell load. From the figure, it can be seen that for cell loads greater than 65 tonnes, corresponding to a sample pressure of 6.81 GPa, the Bragg reflections due to $CuFeS_2$ progressively broaden and diminish in intensity. At the same time, however, the pressure remains essentially constant. At the maximum applied load setting of 90 tonnes, corresponding to a sample pressure of 6.87 GPa, there appears to be no trace of the $CuFeS_2$ powder pattern, the remaining reflections being due to the NaCl pressure marker and contaminant scattering from WC and Ni in the anvils. These results indicate the presence of a phase transition at 6.7(2) GPa to an apparently amorphous phase. The volume change associated with this transformation must be considerable owing to the essentially constant pressure observed during the stepwise increase in cell load from 65 to 90 tonnes. The final pattern collected after careful decompression of the sample back to ambient pressure exhibits several weak and broad peaks indicating a very limited recovery of the original phase of $CuFeS_2$. These results are in good agreement with those reported by Kobayashi *et al*. (2007).

Figure 9a shows the pressure dependence of the lattice parameters between 0.22 and 6.81 GPa. Both a and c show approximately linear decreases with increasing pressure with $-1/a_0\ da/dP = 3.87(3) \times 10^{-3}\ GPa^{-1}$ and $-1/c_0\ dc/dP = 4.45(7) \times 10^{-3}\ GPa^{-1}$. Assuming hydrostatic conditions, the axial compressibilities can be related to the elastic stiffnesses (in Voigt notation), as shown below:

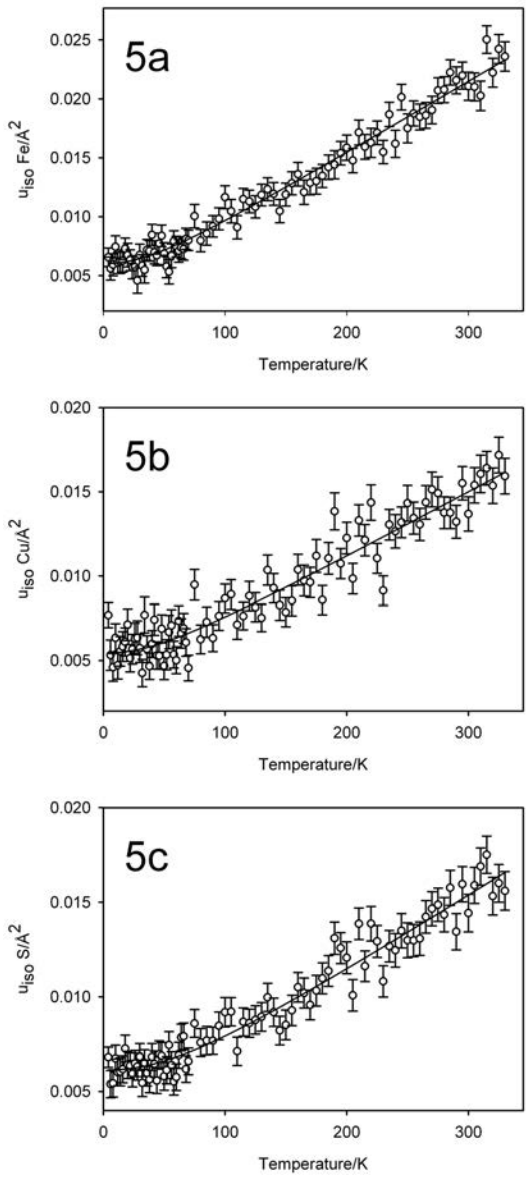

FIG. 5. The temperature variation of the isotropic atomic displacement parameters for Fe (4a), Cu (4b) and S (4c). Full lines show the fits to these data using a modified Debye model.

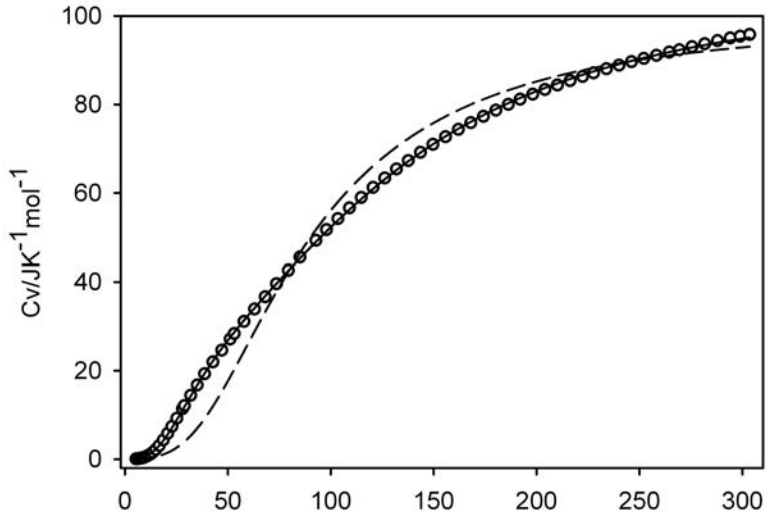

FIG. 6. Isochoric heat-capacity data for synthetic chalcopyrite (Robie *et al*. 1985). The dashed line shows the results of a least-squares fit to a single Debye moment with a derived Debye temperature of 362 K. The full line shows the results of a fit to a two-Debye-moment model with derived Debye temperatures of 167 and 606 K.

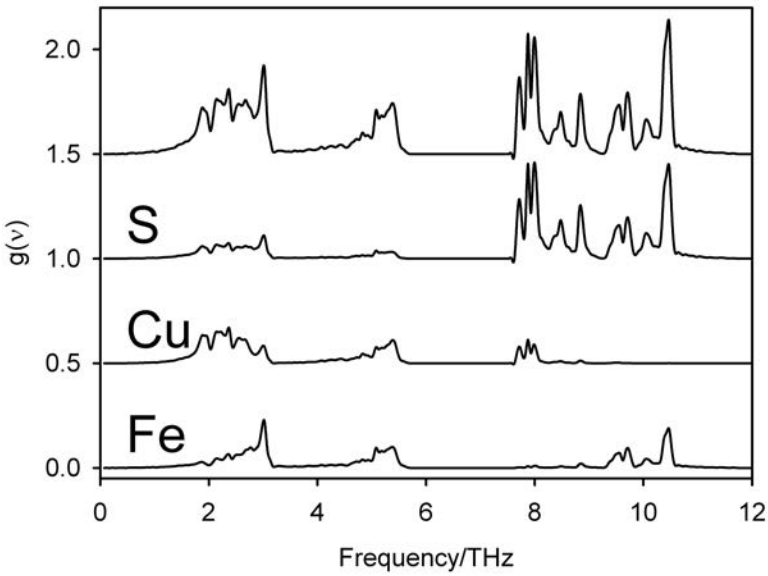

FIG. 7. Calculated partial and total vibrational density of states functions for chalcopyrite (Łażewski *et al*. 2004).

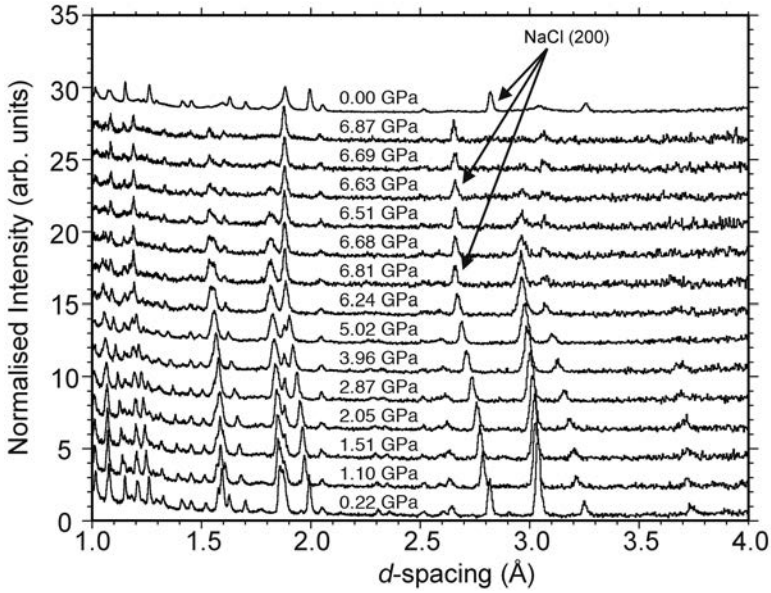

FIG. 8. The observed neutron powder-diffraction patterns obtained on PEARL from the mixed-phase P–E cell loading of $CuFeS_2$ and NaCl. The patterns are shown in the order collected from bottom to top. At the highest load, the only reflections visible are due to the NaCl pressure marker and the WC and Ni from the anvil materials.

$$-\left(\frac{\partial \ln a}{\partial P}\right)_T = \frac{c_{33} - c_{13}}{c_{33}\left(c_{11} + c_{12}\right) - 2c_{13}^2}$$

$$-\left(\frac{\partial \ln c}{\partial P}\right)_P = \frac{c_{11} + c_{12} - 2c_{13}}{c_{33}\left(c_{11} + c_{12}\right) - 2c_{13}^2}.$$

On the basis that the sample reflections only broaden at the amorphization transition, we deduce that the conditions at which the high-pressure data for the tetragonal phase were collected were close to being hydrostatic at all pressures. The calculated axial compressibilities based on the elastic stiffnesses derived from the *ab initio* simulations (Łażewski *et al*. 2004), or X-ray diffraction data (Sirota & Zhalgasbekova 1991), are in poor agreement with our experimental determinations. The calculated elastic stiffnesses overestimate $-\left(\frac{\partial \ln a}{\partial P}\right)_T$ (5.2×10^{-3} GPa^{-1}) and underestimate $-\left(\frac{\partial \ln c}{\partial P}\right)_T$ (3.3×10^{-3} GPa^{-1}), whereas the experimentally derived elastic stiffnesses underestimate both axial compressibilities.

The effect of pressure on the unit-cell volume and a third-order Birch–Murnaghan equation of state fit to these data are shown in Figure 9b. The pressure dependence of the normalized unit-cell volume determined by Kobayashi *et al*. (2007) by X-ray diffraction are included in Figure 9b, and are in excellent agreement with the results from PEARL. Applying weighted least-squares to the PEARL results, the bulk modulus has been determined as 77(2) GPa, and its pressure derivative, as 2.0(6). The bulk modulus is in good agreement with the Voigt–Reuss–Hill average of the calculated elastic stiffnesses derived by Łażewski *et al*. (2004), 74 GPa, but in poorer agreement with the experimental determinations made by Tinoco *et al*. (1994), 91(10) GPa, and Kobayashi *et al*. (2007), 69.9(9) GPa. In the former case, we believe that this discrepancy arises primarily because of the low intrinsic resolution of the energy-dispersive technique, which was not capable of resolving the tetragonal distortion present in the powder-diffraction pattern. As Neumann (2004) and Łażewski *et al*. (2004) have already pointed out, the bulk modulus derived from the results of Sirota & Zhalgasbekova (1991), 122 GPa, can be ignored as it is at variance with expectations, and inferences made from all other measurements and calculations.

A typical example of the quality of the Rietveld refinement of $CuFeS_2$ in the Paris–Edinburgh pressure cell is shown in Figure 10 for data collected at collected at 6.35 GPa, 60 tonnes load. For the Shubnikov group $I\bar{4}2d$, with a magnetic ion at either ca1 or ca2 sites, the *hhl* reflections with $2h + l = 4n$ are purely nuclear

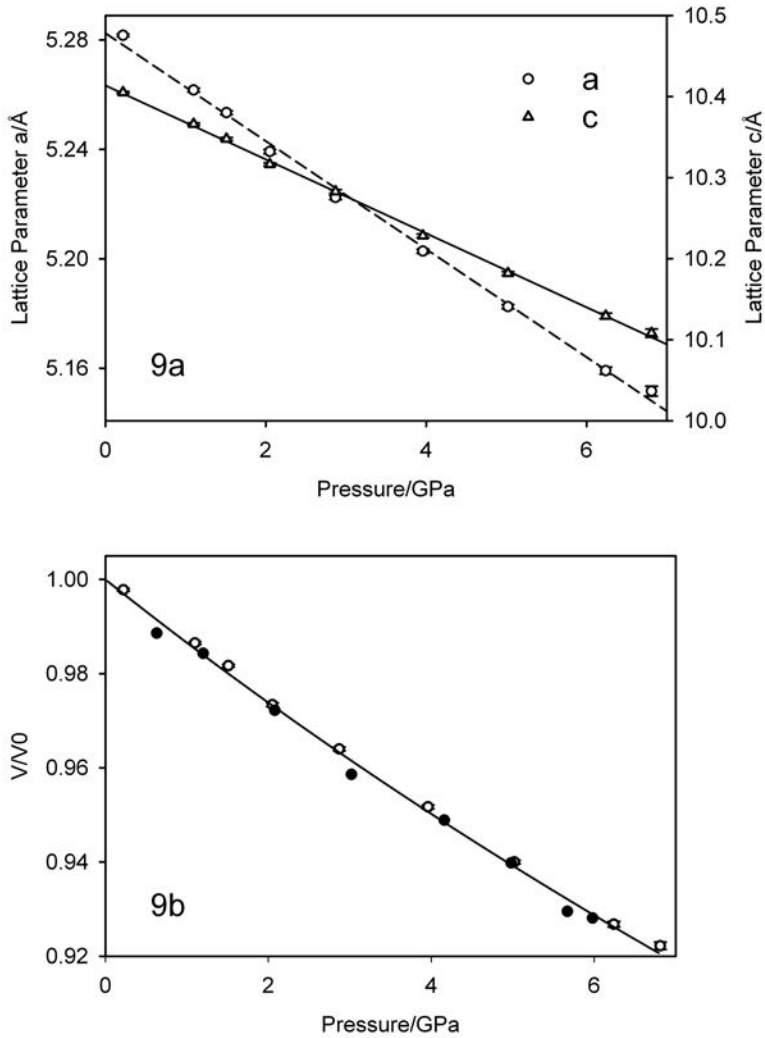

FIG. 9. a. The pressure dependence of the lattice parameters of chalcopyrite. b. The pressure dependence of the normalized volume of chalcopyrite from the PEARL data shown as white circles, with the angle-dispersive X-ray-diffraction data of Kobayashi *et al*. (2007) shown as black circles, for comparison. The full line shows the results of fitting a third-order Birch-Murnaghan equation of state to the PEARL data.

in origin, whereas those with $2h + l = 2n$ are purely magnetic (note that $2h + l = 2n + 1$ is a systematic absence for both classes of reflection). In particular, the strong reflection 110, marked with an arrow on the figure, is purely magnetic in origin, showing that our sample remains a fully compensated antiferromagnet up to the highest pressure measured. This result is in agreement with the Mössbauer results of Boekema *et al*. (2004), but in disagreement with those of Vaughan & Tossell (1973), who found chalcopyrite to become increasingly magnetically disordered from 1 GPa, and to become paramagnetic at pressures of the order of 2 GPa. The samples of Vaughan & Tossell and Boekema *et al*. are both synthetic, whereas our sample is natural; hence we cannot simply dismiss the differences in the magnetic behavior by appealing to sample provenance. It is therefore clear that a systematic study of the electrical and magnetic properties of chalcopyrite is necessary.

The Grüneisen parameters

Using our experimentally determined bulk modulus allows the Grüneisen parameter to be determined for the two vibrational density of states models, and the temperature dependence of the thermodynamic Grüneisen parameter, γ^{th}, to be calculated. For the Einstein model, $\gamma_1' = 1.63(3)$ and $\gamma_2' = -0.5(2)$, and for the Debye model, the corresponding values are $\gamma_1' = 1.81(3)$ and $\gamma_2' = -0.8(1)$. Figure 11 shows the temperature variation of the thermodynamic Grüneisen parameter evaluated using the corrected heat-capacity data of Robie *et al*. (1985) and the thermal expansion coefficient derived from the Debye model fit to the temperature dependence of the unit-cell volume. The alternative abscissa is shown normalized to θ_0, the Debye temperature as $T \rightarrow 0$ K, which for this diagram has been estimated at 230 K from the gradient of a plot of C_V/T *versus* T^2. The results show that γ^{th} is negative for $T < 100$ K, exhibits a minimum at T/θ_0 of approximately 0.055, and has a high-temperature limit of ~0.7. These observations are in excellent agreement with the other adamantine-structured compounds that have been studied at low temperature, Ge, GaAs, ZnSe, ZnS, CdTe, HgTe and CuCl (Barron *et al*. 1980, and references therein). Results from these compounds characteristically show that γ has a minimum for a T/θ_0 of about 0.06 and, for $T \geq \theta_D$, γ lies between 0.6 and 0.8.

Discussion

The low-temperature thermoelastic properties of chalcopyrite have been successfully characterized using neutron powder diffractometry, an analysis of heat-capacity data, and by comparison with the results of *ab initio* calculations. The volume expansivity and heat capacity at constant pressure, analyzed in terms of a two-moment Debye model, have yielded characteristic temperatures, which are gratifyingly close. The lower characteristic temperature is associated with a negative Grüneisen parameter and relates to the excitation of acoustic or quasi-acoustic modes with wave normals [110] and ~[201], which give rise to negative thermal expansion along both axes. The higher characteristic temperature lies above the calculated cut-off frequency in the calculated phonon density of states function, but probably is related to optic modes involving the sulfur in particular. An alternative analysis of the heat capacity as the sum of two Einstein oscillators is in good agreement with the position of the two strongest bands of modes in the calculated vibrational density of states. In contrast, the analysis of the atomic displacement parameters within a modified Debye formalism gave vibrational Debye temperatures that show no direct relationship to the individual partial phonon densities of states. The temperature dependence of the thermodynamic Grüneisen parameter has been determined

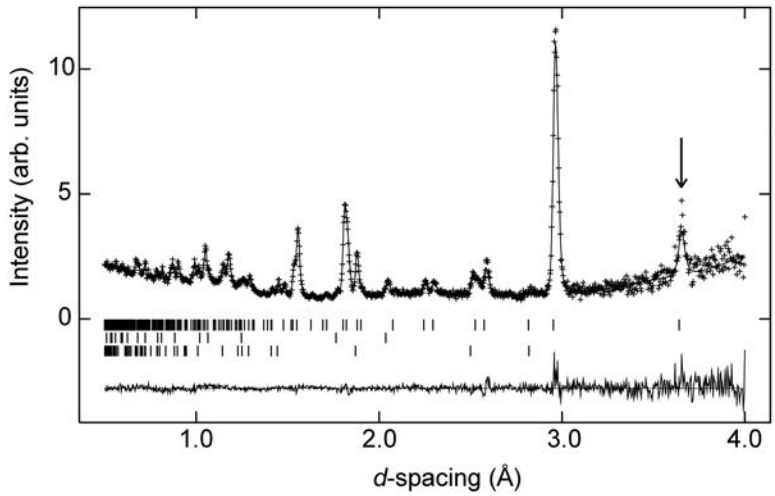

FIG. 10. Final Rietveld refinement plot of chalcopyrite at 6.35 GPa with the purely magnetic reflection 110 arrowed. The presence of the 110 reflection throughout the pressure range studied shows that this sample of chalcopyrite retains the magnetic structure shown in Figure 1 to close to the rock-salt transition pressure. The upper tick marks indicate the chalcopyrite reflections, the middle and lower tick marks, for nickel and tungsten carbide, respectively, show contaminant reflections derived from the anvil materials.

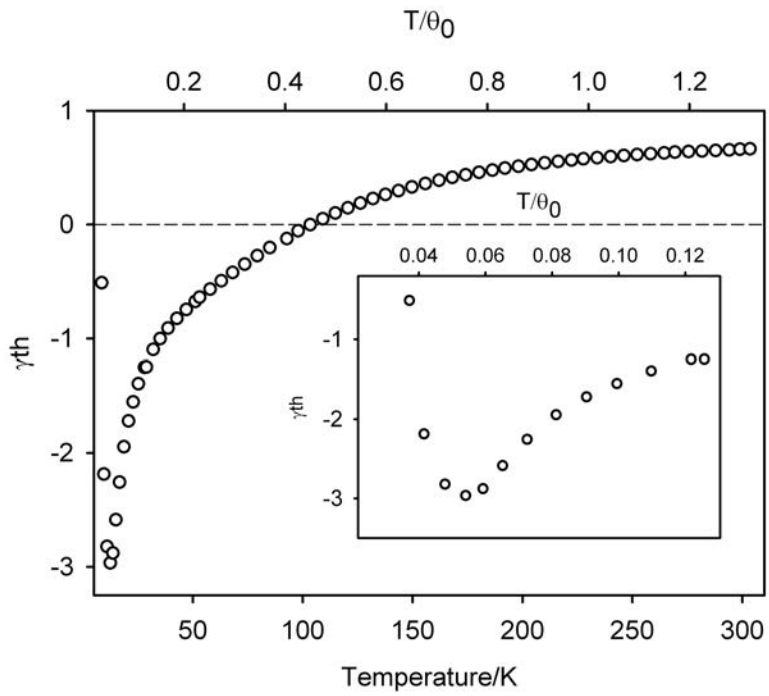

FIG. 11. The temperature variation of the thermodynamic Grüneisen parameter showing typical adamantine behavior: it is negative below 100 K, has a high-temperature limit of ~0.7, and a minimum at T/ θ_0 close to 0.055.

for a chalcopyrite-structured material for the first time and shows that the characteristic adamantine-structure behavior previously observed in group IV and I–VII, II–VI and III–V compounds transfers directly to the I–III–VI_2 ternary compounds.

The measured bulk modulus of chalcopyrite is in excellent agreement with the Voigt–Reuss–Hill average of the calculated elastic constants, but the axial compressibilities based on the same elastic stiffnesses are in relatively poor agreement with experiment. A direct experimental determination of the elastic constants to compare with the results of the calculations would be timely to see where this discrepancy arises.

The room-temperature data have confirmed the magnetic structure originally determined by Donnay *et al.* (1958); however, data collected at 4.2 K have not allowed an unambiguous answer to whether the copper ion orders magnetically below the anomaly seen in the magnetic susceptibility. The magnetic ordering of the copper ion below 50 K would be most easily studied using the element-specific technique of X-ray dichroism, either circular dichroism to probe for ferromagnetic coupling, or linear dichroism to search for antiferromagnetic coupling (Collins *et al.* 2007).

ACKNOWLEDGEMENTS

We are grateful to Richard Pattrick (University of Manchester) for the provision of the sample, and to Michael Henderson (University of Manchester) for the electron-microprobe analysis. Dr. Jan Łażewski (Institute of Nuclear Physics, Cracow) kindly provided the full and partial phonon density of states data for incorporation into Figure 7; we acknowledge useful discussions with Ian Wood and Alex Lindsay-Scott (University College, London) and Kate Wright (Curtin University). High-quality experimental support was provided by Richard Down and Duncan Francis (ISIS Facility). We have benefitted from the constructive comments from two anonymous referees, and we are grateful to Dr. Allen Pratt and Prof. Robert F. Martin for the editorial handling of our manuscript.

REFERENCES

AUSTIN, I.G., GOODMAN, C.H.L. & PENGELLY, A.E. (1956): New semiconductors with the chalcopyrite structure. *J. Electrochem. Soc.* **103**, 609-610.

BARRERA, G.D., BRUNO, J.A.O., BARRON, T.H.K. & ALLAN, N.L. (2005): Negative thermal expansion. *J. Phys.: Condensed Matter* **17**, R217-R252.

BARRON, T.H.K. (1957): Grüneisen parameters for the equation of state of solids. *Annals of Physics* **1**, 77-90.

BARRON, T.H.K., COLLINS, J.G. & WHITE, G.K. (1980): Thermal expansion of solids at low temperatures. *Advances in Physics* **29**, 609-730.

BARRON, T.H.K. & WHITE, G.K. (1999): *Heat Capacity and Thermal Expansion at Low Temperatures*. Kluwer Academic / Plenum Publishers, New York, N.Y.

BESSON, J.M., NELMES, R.J., HAMEL, G., LOVEDAY, J.S., WEILL, G. & HULL, S. (1992): Neutron powder diffraction above 10 GPa. *Physica B* **180–181**, 907-910.

BLACKMAN, M. (1958): On negative volume expansion coefficients. *Phil. Mag.* **3**, 831-838.

BOEKEMA, C., KRUPSKI, A.M., VARASTEH, M., PARVIN, K., VAN TIL, F., VAN DER WOUDE, F. & SAWATZKY, G.A. (2004): Cu and Fe valence states in $CuFeS_2$. *J. Magnetism and Magnetic Materials* **272–276**, 559-561.

BOLTAKS, B.I. & TARNOVSKII, N.N. (1955): The electrical properties of chalcopyrite: effect of surface treatment on the rectifying properties of crystals. *Zh. Teknicheskoi Fiziki* **25**, 402-409 (in Russian).

BRAND, H.E.A., FORTES, A.D., WOOD, I.G., KNIGHT, K.S. & VOČADLO, L. (2009): The thermal expansion and crystal structure of mirabilite (Na_2SO_4•$10D_2O$) from 4.2 to 300 K, determined by time-of-flight neutron powder diffraction. *Phys. Chem. Minerals* **36**, 29-46.

BRÜHL, H.-G., NEUMANN, H., PFEIFFER, T. & KÜHN, G. (1981): Anisotropic thermal expansion of Cu-III-VI_2 compounds. *Physica Status Solidi* (a) **66**, 597-600.

COLLINS, S.P., LOVESEY, S.W. & BALCAR, E. (2007): Dichroism and resonant diffraction in X-ray scattering by complex materials. *J. Phys.: Condensed Matter* **19**, 213201.

DECKER, D.L. (1971): High-pressure equation of state for NaCl, KCl and CsCl. *J. Appl. Phys.* **42**, 3239-3244.

DEUS, P., NEUMANN, H., KÜHN, G. & HINZE, B. (1983): Low-temperature thermal expansion of $CuInSe_2$. *Physica Status Solidi* (a) **80**, 205-209.

DEUS, P., VOLAND, U. & NEUMANN, H. (1988): Low-temperature thermal expansion of $ZnSiAs_2$. *Physica Status Solidi* (a) **108**, 225-231.

DONNAY, G., CORLISS, L.M., DONNAY, J.D.H., ELLIOTT, N. & HASTINGS, J.M. (1958): Symmetry of magnetic structures: magnetic structure of chalcopyrite. *Phys. Rev.* **112**, 1917-1923.

DONOVAN, B. & REICHENBAUM, G. (1958): Electrical properties of chalcopyrite. *Brit. J. Appl. Phys.* **9**, 474-477.

ENGIN, T.E., POWELL, A.V., HAYNES, R., CHOWDHURY, M.A.H., GOODWAY, C.M., DONE, R., KIRICHEK, O. & HULL, S. (2008): A high temperature cell for simultaneous electrical resistance and neutron diffraction measurements. *Rev. Sci. Instrum.* **79**, 095104.

ENGIN, T.E., POWELL, A.V. & HULL, S. (2011): A high temperature diffraction-resistance study of chalcopyrite, $CuFeS_2$. *J. Solid State Chem.* **184**, 2272-2277.

FATELEY, W.G., DOLLISH, F.R., MCDEVITT, N.T. & BENTLEY, F.F. (1972): *Infrared and Raman Selection Rules for Molecular and Lattice Vibrations: the Correlation Method*. Wiley Interscience, New York, N.Y.

FORTES, A.D., WOOD, I.G., ALFREDSSON, M., VOČADLO, L. & KNIGHT, K.S. (2005): The incompressibility and thermal expansivity of D_2O ice II determined by powder neutron diffraction. *J. Appl. Crystallogr.* **38**, 612-618.

FORTES, A.D., WOOD, I.G., ALFREDSSON, M., VOČADLO, L. & KNIGHT, K.S. (2006): The thermoelastic properties of $MgSO_4$•$7D_2O$ (epsomite) from powder neutron diffraction and *ab initio* calculation. *Eur. J. Mineral.* **18**, 449-462.

FOURET, R., DEROLLEZ, P., LAAMYEM, A., HENNION, B. & GONZALEZ, J. (1997): Phonons in silver gallium diselenide. *J. Phys.: Condensed Matter* **9**, 6579-6589.

GOPAL, E.S.R. (1966): *Specific Heats at Low Temperatures*. Heywood Books, London, U.K.

GORBUNOVA, I.E., GROGORYEVA, V.M., TSEMEKHMAN, L.S., IVANCHENKO, L.P. & SHISHKIN, N.N. (1978): Behaviour of chalcopyrite during heating in various atmospheres. *Izvestiya Rossiiskoi akademii nauk. Metally* **6**, 22-25 (in Russian).

GRIMVALL, G. (1999): *Thermophysical Properties of Materials*. North Holland – Elsevier, Amsterdam, The Netherlands.

HAILING, T., SAUNDERS, G.A., LAMBSON, W.A. & FEIGELSON, R.S. (1982): Elastic behaviour of the chalcopyrite $CdGeAs_2$. *J. Phys. C: Solid State Phys.* **15**, 1399-1418.

HAMAJIMA, T., KAMBARA, T. & GONDAIRA, K.I. (1981): Self-consistent electronic structures of magnetic semiconductors by a discrete variational *X*α calculation. III. Chalcopyrite $CuFeS_2$. *Phys. Rev. B* **24**, 3349-3353.

HARRIS, M.J., ZINKIN, M.P. & SWAINSON, I.P. (1997): Phonons and spin waves in the magnetic semiconductor chalcopyrite, $CuFeS_2$. *Phys. Rev. B* **55**, 6957-6959.

KNIGHT, K.S. & HENDERSON, C.M.B. (2007): Structural basis for the low-temperature thermal expansion of the gillespite-structured phase $Ba_{0.5}Sr_{0.5}CuSi_4O_{10}$. *Eur. J. Mineral.* **19**, 189-200.

KNIGHT, K.S. & PRICE, G.D. (2008): Powder neutron-diffraction studies of clinopyroxenes. I. The crystal structure and thermoelastic properties of jadeite between 1.5 and 270 K. *Can. Mineral.* **46**, 1593-1622.

KOBAYASHI, H., UMEMURA, J., KAZEKAMI, Y., SAKAI, N., ALFÈ, D., OHISHI, Y. & YODA, Y. (2007): Pressure-induced amorphization of $CuFeS_2$ studied by ^{57}Fe nuclear resonant inelastic scattering. *Phys. Rev. B* **76**, 134108.

KRADINOVA, L.V., POLUBOTKO, A.M., POPOV, V.V., PROCHUKHAN, V.D., RUD, Y.V. & SKORYUKIN, V.E. (1987): Low-temperature electronic-properties of $CuFeS_2$ and its band diagram at the point Γ. *Fizika Tverdogo Tela* **29**, 2209-2213.

LARSON, A.C. & VON DREELE, R.B. (1986): General Structure Analysis System. *Los Alamos Nat. Lab., Rep.* **LAUR 86-748**.

ŁAŻEWSKI, J., NEUMANN, H. & PARLINSKI, K. (2004): *Ab initio* characterization of magnetic $CuFeS_2$. *Phys. Rev. B* **70**, 195206.

MIKHAILOVSKII, A.P., POLUBOTKO, A.M., PROCHUKHAN, V.D. & RUD, Y.V. (1990): Gapless state in $CuFeS_2$. *Physica Status Solidi* (b) **158**, 229-238.

MIKHLIN, Y., TOMASHEVICH, Y., TAUSON, V., VYALIKH, D., MOLODTSOV, S. & SZARGAN, R. (2005): A comparative X-ray absorption near-edge structure study of bornite, Cu_5FeS_4, and chalcopyrite, $CuFeS_2$. *J. Electron Spectrosc. Related Phenomena* **142**, 83-88.

MUSSEL, W.N., MURAD, E., FABRIS, J.D., MOREIRA, W.S., BARBOSA, J.B.S., MURTA, C.C., ABRAHÃO, W.P., DEMELLO, J.W.V. & GARG, V.K. (2007): Characterization of a chalcopyrite from Brazil by Mössbauer spectroscopy and other physicochemical techniques. *Phys. Chem. Minerals* **34**, 383-387.

NEUMANN, H. (1980): Trends in the thermal expansion coefficients of the $A^IB^{III}C^{VI}_2$ and $A^{II}B^{IV}C^{V}_2$ chalcopyrite compounds. *Kristall und Technik* **15**, 849-857.

NEUMANN, H. (2004): Review: lattice dynamics and related properties of $A^IB^{III}C^{VI}_2$ and $A^{II}B^{IV}C^{V}_2$ compounds. I. Elastic constants. *Crystal Res. Technol.* **39**, 939-958.

NEUMANN, H., DEUS, P., TOMLINSON, R.D., KÜHN, G. & HINTZE, B. (1984): Thermal expansion of $CuInTe_2$ from 30 to 300 K. *Physica Status Solidi* (a) **84**, 87-93.

OGUCHI, T., SATO, K. & TERANISHI, T. (1980): Optical reflectivity spectrum of a $CuFeS_2$ single crystal. *J. Phys. Soc. Japan* **48**, 123-128.

PEARCE, C.I., PATTRICK, R.A.D., VAUGHAN, D.J., HENDERSON, C.M.B. & VAN DER LAAN, G. (2006): Copper oxidation state in chalcopyrite: mixed Cu d^9 and d^{10} characteristics. *Geochim. Cosmochim. Acta* **70**, 4635-4642.

PIEKOSZEWSKI, J., SUWALSKI, J. & LIGENZA, S. (1968): Mössbauer effect study in chalcopyrite. *Physica Status Solidi* (*b*) **29**, K99-K101.

PITT, G.D. & VYAS, M.K.R. (1974): Metal–semiconductor transition in single crystal chalcopyrite ($CuFeS_2$). *Solid State Commun.* **15**, 899-902.

PRIDMORE, D.F. & SHUEY, R.T. (1976): The electrical resitivity of galena, pyrite and chalcopyrite. *Am. Mineral.* **61**, 248-259.

ROBIE, R.A., WIGGINS, L.B., BARTON, P.B., JR. & HEMINGWAY, B.S. (1985): Low-temperature heat-capacity and entropy of chalcopyrite ($CuFeS_2$): estimates of the standard molar enthalpy and Gibbs free energy of formation of chalcopyrite and bornite (Cu_5FeS_4). *J. Chem. Thermodynamics* **17**, 481-488.

ROBINSON, K., GIBBS, G.V. & RIBBE, P.H. (1971): Quadratic elongation: a quantitative measure of distortion in coordination polyhedra. *Science* **172**, 567-570.

SHAY, J.L. & WERNICK, J.H. (1975): *Ternary Chalcopyrite Semiconductors, Growth, Electronic Properties and Applications*. Pergamon Press, Oxford, U.K.

SIROTA, N.N. & ZHALGASBEKOVA Z.K. (1991): Elastic stiffness constants of chalcopyrite from X-ray diffraction analysis. *Dokl. Akad. Nauk SSSR* **321**, 513-517.

STOKES, H.T. & HATCH, D.M. (1988): *Isotropy Subgroups of the 230 Crystallographic Space Groups*. World Scientific, Singapore.

TERANISHI, T. (1961): Magnetic and electric properties of chalcopyrite. *J. Phys. Soc. Japan* **16**, 1881-1887.

TINOCO, T., ITIÉ, J.P., POLIAN, A., SAN MIGUEL, A., MOYA, E., GRIMA, P., GONZALEZ, J. & GONZALEZ, F. (1994): Combined X-ray absorption and X-ray diffraction studies of $CuGaS_2$, $CuGaSe_2$, $CuFeS_2$ and $CuFeSe_2$ under high pressure. *J. de Physique IV, Colloque* **C94**, C9-151-154.

TODD, E.C. & SHERMAN, D.M. (2003): Surface oxidation of chalcocite (Cu_2S) under aqueous (pH = 2–10) and ambient atmospheric conditions: mineralogy from Cu *L*- and O *K*-edge X-ray absorption spectroscopy. *Am. Mineral.* **88**, 1652-1656.

TODD, E.C., SHERMAN, D.M. & PURTON, J.A. (2003): Surface oxidation of chalcopyrite ($CuFeS_2$) under ambient atmospheric and aqueous (pH = 2-11) conditions: Cu, Fe *L*- and O *K*-edge X-ray spectroscopy. *Geochim. Cosmochim. Acta* **67**, 2137-2146.

VAUGHAN, D.J. & TOSSELL, J.A. (1973): Magnetic transitions observed in sulfide minerals at elevated pressures and their geophysical significance. *Science* **179**, 375-377.

WALLACE, D.C. (1972): *Thermodynamics of Crystals.*Wiley, New York, N.Y.

WOOD, I.G., KNIGHT, K.S., PRICE, G.D. & STUART, J.A. (2002): Thermal expansion and atomic displacement parameters of cubic $KMgF_3$ perovskite determined by high-resolution neutron powder diffraction. *J. Appl. Crystallogr.* **35**, 291-295.

WOOD, I.G., VOČADLO, L., KNIGHT, K.S., DOBSON, D.P., MARSHALL, W.G., PRICE, G.D. & BRODHOLT, J. (2004): Thermal expansion and crystal structure of cementite, Fe_3C, between 4 and 600 K determined by time-of-flight neutron powder diffraction. *J. Appl. Crystallogr.* **37**, 82-90.

WOOLLEY, J.C., LAMARCHE, A.-M., LAMARCHE, G., QUINTERO, M., SWAINSON, I.P. & HOLDEN, T.M. (1996): Low temperature magnetic behaviour of $CuFeS_2$ from neutron diffraction data. *J. Magnetism Magnetic Mater.* **162**, 347-354.

Received February 27, 2011, revised manuscript accepted July 19, 2011.